http://dx.doi.org/10.5012/bkcs.2011.32.9.3453

Composition Dependence on Structural and Optical Properties of $Mg_xZn_{1-x}O$ Thin Films Prepared by Sol-Gel Method

Min Su Kim,[†] Keun Tae Noh,[‡] Kwang Gug Yim,[†] Soaram Kim,[‡] Giwoong Nam,[‡] Dong-Yul Lee,[§] Jin Soo Kim,[#] Jong Su Kim,[¶] and Jae-Young Leem[†,‡,*]

[†]*Department of Nano Systems Engineering, Center for Nano Manufacturing, Inje University, Gimhae Gyungnam 621-749, Korea*
[‡]*School of Nano Engineering, Inje University, Gimhae Gyungnam 621-749, Korea. [*]E-mail: jyleem@inje.ac.kr*
[§]*Epi R&D Team, Samsung LED Co. Ltd., Suwon, Gyeonggi-do 443-373, Korea*
[#]*Research Center of Advanced Materials Development (RCAMD), Division of Advanced Materials Engineering, Chonbuk National University, Jeonju, Chonbuk 561-756, Korea*
[¶]*Department of Physics, Yeungnam University, Gyeongsan, Gyeongsangbuk-do 712-749, Korea*
Received June 29, 2011, Accepted August 1, 2011

The $Mg_xZn_{1-x}O$ thin films with the various content ratio ranging from 0 to 0.4 were prepared by sol-gel spin-coating method. To investigate the effects of content ratio on the structural and optical properties of the $Mg_xZn_{1-x}O$ thin films, scanning electron microscopy (SEM), X-ray diffraction (XRD), and photoluminescence (PL) were carried out. With increase in the content ratio, the grain size of the $Mg_xZn_{1-x}O$ thin films was increased, however, at the content ratio above 0.2, MgO particles with cubic structure were formed on the surface of the $Mg_xZn_{1-x}O$ thin films, indicating that the Mg content exceeded its solubility limit in the thin films. The residual stress of the $Mg_xZn_{1-x}O$ thin films is increased with increase in the Mg mole fraction. In the PL investigations, the bandgap and the activation energy of the $Mg_xZn_{1-x}O$ thin films was increased with the Mg mole fraction.

Key Words : Magnesium, Zinc oxide, Sol-gel method, X-ray diffraction, Photoluminescence

Introduction

ZnO and MgZnO are group II-VI wide-bandgap materials that are currently under intense study as blue and ultraviolet light-emitting diodes (LEDs).[1-5] In particular, its large exciton binding energy of 60 meV,[6] which is larger than the thermal energy at room temperature (RT), allows excitons to play important roles at RT and ensures efficient lasing even at RT.[7] In addition, its high thermal and chemical stability with the possibility of using the wet processing has led to ZnO-based oxide semiconductor as an alternative material to nitride semiconductors.

However, to fully utilize ZnO-based oxide semiconductor in optoelectronic devices, the realization of bandgap engineering is required to grow barrier layers and quantum well in heterostructures. In general, Mg is incorporated as substitutional type materials to control the bandgap in ternary oxide semiconductors.[8,9] Although Mg^{2+} (0.57 Å) has a similar ionic radius to Zn^{2+} (0.60 Å), the solid solubility of MgO in the ZnO matrix is limited due to its different crystal structure. MgO has a cubic rock salt structure,[10] while ZnO has a hexagonal wurtzite structure.[11] So, the reports have demonstrated that the MgZnO alloy thin films with a wide range of Mg^{2+} from 0 to 36% still maintained the hexagonal lattice structure due to the similar ionic radius of Mg^{2+} and Zn^{2+}, and corresponding energy bandgap could be increased from 3.34 to 3.96 eV.[12] Moreover, the MgZnO thin films could produce a bright ultraviolet luminescence at RT due to the band edge exciton recombination. This makes the MgZnO thin films acts as an excellent candidate for ultraviolet optoelectronic devices such as UV LED, UV laser, and UV detector.

Nonequilibrium growth conditions vary with the preparing technique, such as pulsed laser deposition (PLD),[13,14] sputtering,[15] metalorganic vapor phase epitaxy (MOVPE),[16] and molecular beam epitaxy (MBE),[17] leading to a different Mg saturation concentration. Accordingly, it is worth applying various preparation methods to explore the Mg saturation content and thermal stability of the MgZnO alloys in order to better understand this material. Until now, little work has been done to investigate the MgZnO thin films by using sol-gel method.[18] In this study, sol-gel spin-coating method was adopted to deposit the $Mg_xZn_{1-x}O$ thin films with various Mg mole fractions because spin-coating technique has distinct advantages such as easy and cheap operation, excellent compositional control, and homogeneity on the molecular level.

Experimental Details

The $Mg_xZn_{1-x}O$ thin films were grown on Si (100) substrates by using sol-gel spin-coating method. The Si substrates were cleaned by immersion in a piranha solution (H_2SO_4:H_2O_2 = 8:1) at 110 °C for 15 min and then in hydrofluoric acid (HF 50%:H_2O = 1:9) for 1 min. The preparation of the $Mg_xZn_{1-x}O$ thin films is illustrated schematically in Figure 1. The precursor solution was prepared by dissolving 0.5 M zinc acetate dihydrate [$Zn(CH_3COO)_2{\cdot}2H_2O$] in

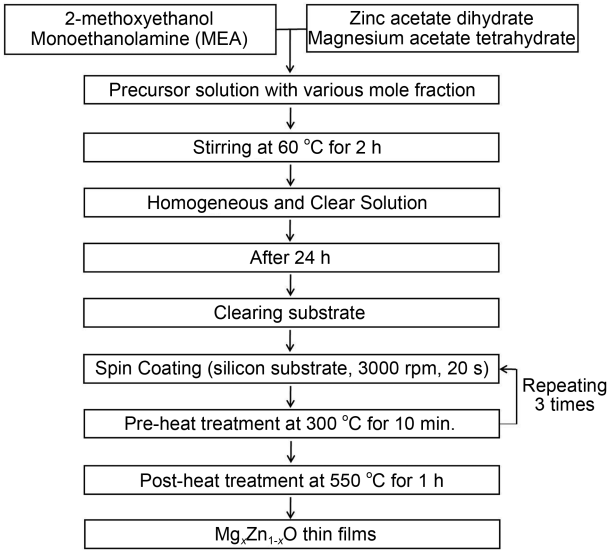

Figure 1. Flow chart for the preparation of the $Mg_xZn_{1-x}O$ thin films by sol-gel spin-coating method.

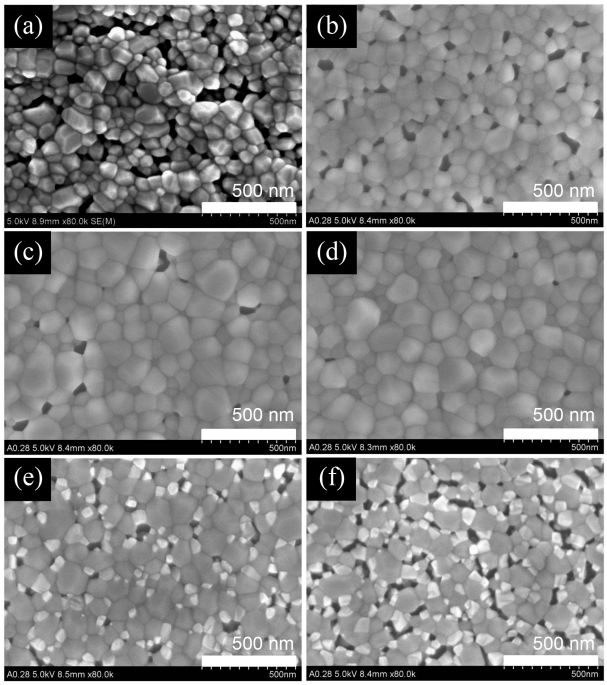

Figure 2. SEM images of the $Mg_xZn_{1-x}O$ thin films with various content ratio of magnesium acetate tetrahydrate to zinc acetate dihydrate; (a) 0, (b) 0.05, (c) 0.1, (d) 0.2, (e) 0.3, and (f) 0.4.

0.5 M 2-methoxyethanol as a solvent, and monoethanolamine (MEA) was added to the stable sol solution. The molar ratio of zinc acetate dihydrate to 2-methoxyethanol was maintained at 1:1. The Mg mole fraction was controlled by the change in the wt % ratio of magnesium acetate tetrahydrate [$Mg(CH_3COO)_2{\cdot}4H_2O$] to zinc acetate dihydrate from 0 to 0.4. The resultant sol solution was stirred at 60 °C for 2 h to yield a clear and homogenous solution. The sol solution was preserved for 1 day before the growth of the $Mg_xZn_{1-x}O$ thin films. The sol solution was spin-coated onto Si substrate, rotated at 3000 rpm for 20 s. The $Mg_xZn_{1-x}O$ thin films were heated at 300 °C for 10 min to evaporate the solvent and remove the organic residuals (named as pre-heat treatment). After the pre-heat treatment, the $Mg_xZn_{1-x}O$ thin films were cooled with the cooling rate of 5 °C/min to avoid cracks. The spin-coating and pre-heating processes were repeated three times. In order to crystallize, the $Mg_xZn_{1-x}O$ thin films were heated in a furnace under an air atmosphere at 500 °C for 1 h (named as post-heat treatment). The effects of Mg mole fraction on the structural and the optical properties of the $Mg_xZn_{1-x}O$ thin films were investigated by scanning electron microscopy (SEM), X-ray diffraction (XRD), and photoluminescence (PL).

Results and Discussion

Figure 2 shows SEM images of the $Mg_xZn_{1-x}O$ thin films with different content ratio of magnesium acetate tetrahydrate to zinc acetate dihydrate; (a) 0, (b) 0.05, (c) 0.1, (d) 0.2, (e) 0.3, and (f) 0.4. All the $Mg_xZn_{1-x}O$ thin films exhibit a rough surface with the three-dimensional (3D) island growth. In the initial stage of ZnO thin films growth on Si substrates, ZnO thin films generally show 3D islands[19] due to the lattice and chemical mismatches between the ZnO and the Si. These factors make the surface of the ZnO films on Si rough. The number of the voids was decreased with increase in the content ratio of the $Mg_xZn_{1-x}O$ thin films. The incorporation of Mg in MgZnO thin films may promote lateral growth and favor layer-by-layer growth with smooth surface in comparison to the ZnO thin films on Si as the increase in the Mg content. In the ZnO thin films with a hexagonal wurtzite structure, the preferred growth direction is along the *c*-axis with [001] crystal orientation. Thus, the vertical growth rate is rapid with the relatively limited lateral growth.[20] However, the addition of MgO with a cubic rock salt structure suppresses the vertical growth along the [001] direction and promotes the lateral growth. Consequently, this leads increase in the particle density of the $Mg_xZn_{1-x}O$ thin films. The void was gradually increased by further increase in the content ratio. In addition, the particles were formed due to relatively high content ratio.[21]

Figure 3 shows the XRD patterns of the $Mg_xZn_{1-x}O$ thin films with different content ratio of magnesium acetate tetrahydrate to zinc acetate dihydrate. From all the $Mg_xZn_{1-x}O$ thin films, four ZnO diffraction peaks at 31°, 34°, 36°, and 56° are observed, corresponding to ZnO (100), (002), (101), and (110), respectively. The intensity of the diffraction peak at 34° from the MgZnO thin films ($0.05 \le x \le 0.4$) is stronger than that of the ZnO, which indicates that preferred growth direction is along the *c*-axis with [001] crystal orientation. It is well-known that ZnO is usually grown with *c*-axis preferred orientation under typical growth conditions because of the lowest surface energy of the (001) basal plane in ZnO, leading to a preferred growth in the [001] direction.[22] In general, the intensity of the (002) diffraction peak of $Mg_xZn_{1-x}O$ films was decreased with increase in the Mg content due to the degraded crystallographic characteri-

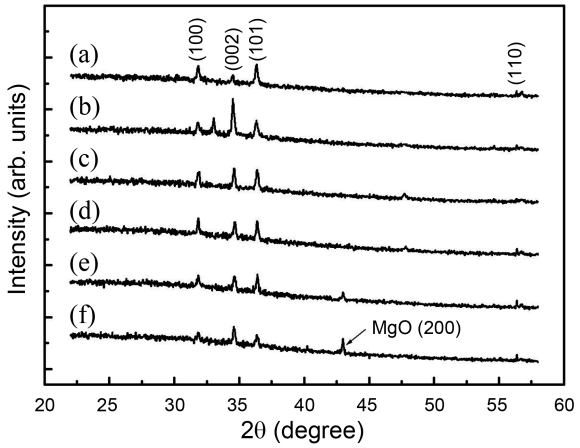

Figure 3. XRD pattern of the $Mg_xZn_{1-x}O$ thin films with various content ratio of magnesium acetate tetrahydrate to zinc acetate dihydrate; (a) 0, (b) 0.05, (c) 0.1, (d) 0.2, (e) 0.3, and (f) 0.4.

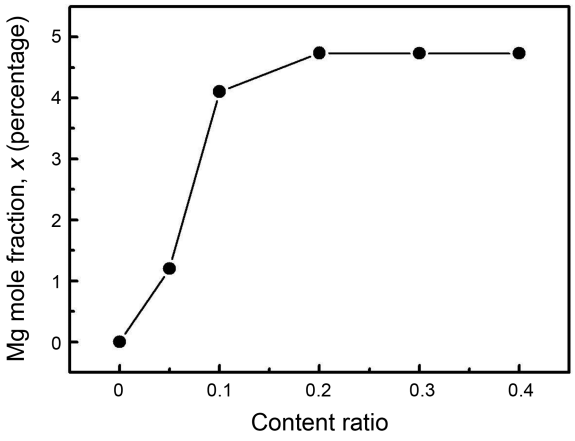

Figure 4. Mg mole fraction of the $Mg_xZn_{1-x}O$ thin films as a function of the content ratio of magnesium acetate tetrahydrate to zinc acetate dihydrate.

stics.[23] However, the opposite results were occasionally reported.[24,25] It was assumed that the enhancement in the (002) diffraction peak was due to increase in the oxygen affinity between Zn and O caused by the incorporation of MgO. The dynamic affinity of the Zn for bonding with O might be improved by the incorporation with a suitable amount of MgO due to the oxygen affinity of the Mg is larger than that of the Zn. The relatively stronger bond between Mg and O leads to the existence of more oxygen, in sequence, the more stoichiometric ZnO crystals were generated in the $Mg_xZn_{1-x}O$ thin films. As a result, the intensity of the (002) diffraction peak from the $Mg_xZn_{1-x}O$ thin films with the Mg content ratio of 0.05 was much stronger than that of the ZnO. However, the intensity of the (002) diffraction peak was again decreased further increase in the content ratio, which was because the influence of the degraded crystallographic characteristics became larger than that of the stoichiometric improvement. To demonstrate that further studies will be needed. The formation of MgO on surface of the MgZnO thin films was observed as evidenced by the appearance of MgO (200) diffraction peak at 43°, indicating that the Mg content exceeded its solubility limit in the MgZnO alloys.

The lattice parameters of the $Mg_xZn_{1-x}O$ thin films vary with the composition by following Vegard's law, showing a linear relationship among them. With $d(002)_{ZnO}$ = 2.6065 Å and $d(111)_{MgO}$ = 2.4363 Å, the lattice parameters of the $Mg_xZn_{1-x}O$ thin films change by following linear expression,

$$d(Mg_xZn_{1-x}O) = d(111)_{MgO}\cdot x + d(002)_{ZnO}\cdot(1\text{-}x) \quad (1)$$

Therefore, the average Mg mole fraction in the $Mg_xZn_{1-x}O$ thin films estimated from above equation for the ZnO (002) diffraction peak position is 0%, 1.2%, 4.1%, 4.7%, 4.7%, and 4.7% for the content ratio of 0, 0.05, 0.1, 0.2, 0.3, and 0.4, respectively. Figure 4 shows the average Mg mole fraction as a function of the content ratio of magnesium acetate tetrahydrate to zinc acetate dihydrate. At the content ratio above 0.2, the Mg mole fraction is almost same, which indicates that the solid solubility of the $Mg_xZn_{1-x}O$ thin films grown by sol-gel spin-coating method is limited at the content ratio of 0.2 (average Mg mole fraction: 4.7%). According to the phase diagram of the ZnO-MgO binary system, the thermodynamic solubility limit of MgO in ZnO is about 4 at %, due to the different crystal structures of ZnO and MgO. However, Ohtomo *et al.*[13] suggested that the solid solubility of MgO in ZnO prepared by PLD is 33% for thin films alloys under metastable conditions. Yang *et al.*[14] also reported the complete bandgap alloying of $Mg_xZn_{1-x}O$ prepared by PLD for the Mg mole fraction ranging from 0 to 1. The $Mg_xZn_{1-x}O$ with the Mg mole fraction in the range from 0 to 0.37 has a hexagonal wurtzite structure. At the Mg mole fraction ranging from 0.37 to 0.62, $Mg_xZn_{1-x}O$ has a mixed structure of hexagonal and cubic phases with undefined energy bandgap. By further increase in the Mg mole fraction, $Mg_xZn_{1-x}O$ has a cubic structure. In the PLD growth process, the precursors arrive at the substrate surface and rapidly cooled. So, the nonequilibrium nature of crystal growth enabled to fabricate solid solution MgZnO thin films well above the thermodynamic solubility limit.[13] However, the solubility limit of MgO in ZnO for the MgZnO thin films in this study was 4.7% because the sol-gel spin-coating method is performed under equilibrium nature of crystal growth.

Figure 5 shows the residual stress and the bond length as a function of the content ratio of magnesium acetate tetrahydrate to zinc acetate dihydrate. The residual stress σ in the $Mg_xZn_{1-x}O$ thin films can be expressed as[26]

$$\sigma = \frac{2C_{13}^2 - C_{33}(C_{11}+C_{12})}{2C_{13}} \times \frac{c-c_0}{c_0} \quad (2)$$

where C_{ij} are elastic stiffness constants for ZnO (C_{11} = 207.0 GPa, C_{33} = 209.5 GPa, C_{12} = 117.7 GPa, and C_{13} = 106.1 GPa). The c and the c_0 are the lattice parameters of the ZnO thin films and of the strain-free ZnO, respectively. If the stress is positive, the biaxial stress is tensile; if the stress is negative, the biaxial stress is compressive. The residual

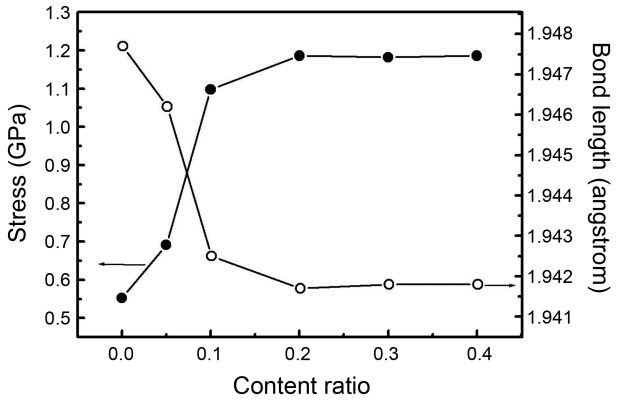

Figure 5. Residual stress and bond length of Zn-O in the $Mg_xZn_{1-x}O$ thin films as a function of the content ratio of magnesium acetate tetrahydrate to zinc acetate dihydrate.

stress of the $Mg_xZn_{1-x}O$ thin films was increased as the content ratio was increased, however, it was keep constant at the content ratio above 0.2 due to the saturation of Mg incorporation. This tendency is very similar to the change in Mg mole fraction as shown in Figure 4. The residual stress is generated in the ZnO due to the difference in the lattice constants and the thermal expansion coefficients between ZnO and Si. For the $Mg_xZn_{1-x}O$ thin films, the residual stress was increased with increase in the Mg mole fraction due to the difference ionic radius and the lattice distortion. The bond length L of the Zn-O is given by

$$L = \sqrt{\left(\frac{a^2}{3} + \left(\frac{1}{2} - u\right)^2 c^2\right)} \quad (3)$$

where the u parameter is given by (in the wurtzite structure)

$$u = \frac{a^2}{3c^2} + 0.25 \quad (4)$$

and relates to a/c ratio. The bond length of the Zn-O in the $Mg_xZn_{1-x}O$ thin films was decreased from 1.948 to 1.942 Å at the content ratio ranging from 0 to 0.2. By further increase in the content ratio, the bond length is almost same due to saturated Mg incorporation.

Figure 6 shows normalized PL spectra of (a) near-band-edge emission (NBE) and (b) deep-level emission (DLE) peak of the $Mg_xZn_{1-x}O$ thin films. Figure 6(c) exhibits the energy of NBE and DLE peak as a function of the content ratio and the inset shows the residual stress as a function of the NBE peak energy. The PL spectra of the $Mg_xZn_{1-x}O$ thin films have typical emissions in UV and visible ranges. In the UV range, NBE peak is generated by the free-exciton recombination, but in the visible range, DLE peak is caused by impurities and structural defects such as oxygen vacancies and zinc interstitials. As shown in Fig. (a) and (c), the NBE peak was shifted to high-energy site as the content ratio increased from 0 to 0.2, which corresponds to an increase in the bandgap from 3.28 to 3.47 eV, and a further increase in the content ratio, however, rarely changed NBE peak energy. This provides an evidence for the saturation of Mg content

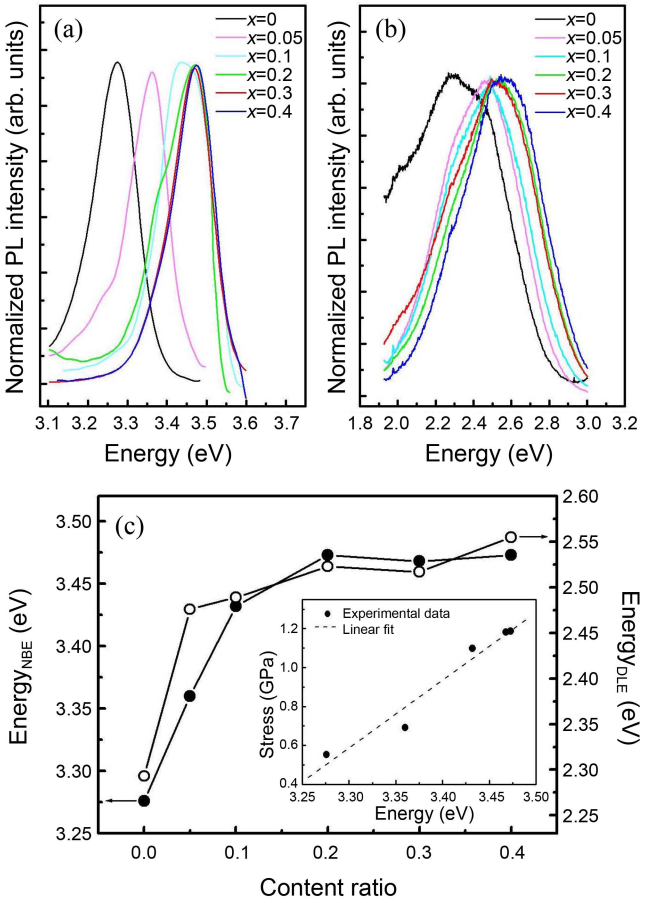

Figure 6. Normalized PL spectra of (a) near-band-edge emission (NBE) and (b) deep-level emission (DLE) peak of the $Mg_xZn_{1-x}O$ thin films. (c) shows energy of NBE and DLE peak as a function of the content ratio and the inset exhibits the residual stress as a function of the NBE peak energy.

in the $Mg_xZn_{1-x}O$ thin films grown by sol-gel spin-coating method. On the other hand, the energy of the DLE peak was increased from 2.29 to 2.56 eV as the content ratio increased up to 0.4. This is because the origin of the DLE peak is band-to-deep level radiative recombination while the NBE peak is caused by band-to-band radiative recombination in ZnO. Nonlinear optical properties related to band gap of sol-gel $Mg_xZn_{1-x}O$ thin films as a function of Mg content were reported by Ghosh and Basak.[27] The green emission of ZnO (content ratio: 0) has been attributed to various types of defects such as oxygen vacancies (V_O),[28] zinc vacancies (V_{Zn}),[29] oxygen atoms at the zinc position in the crystal lattice (O_{Zn}),[19] as well as donor-acceptor pair (DAP).[30] However, there are only few reports for the effects of Mg mole fraction on defect-related PL of $Mg_xZn_{1-x}O$ thin films. Trunk *et al.*[31] suggested that the blue emission of $Mg_xZn_{1-x}O$ thin films is attributed to transitions of interstitial zinc (Zn_i) to V_{Zn} and Zn_i to interstitial oxygen (O_i). And also, the green emission of $Mg_xZn_{1-x}O$ thin films is caused by free-to-bound type transitions between Zn_i/V_{Zn} with E_V/E_C edges, respectively. Ogawa and Fujihara[32] reported that the blue emission of $Mg_xZn_{1-x}O$ thin films is related to increase in the bandgap

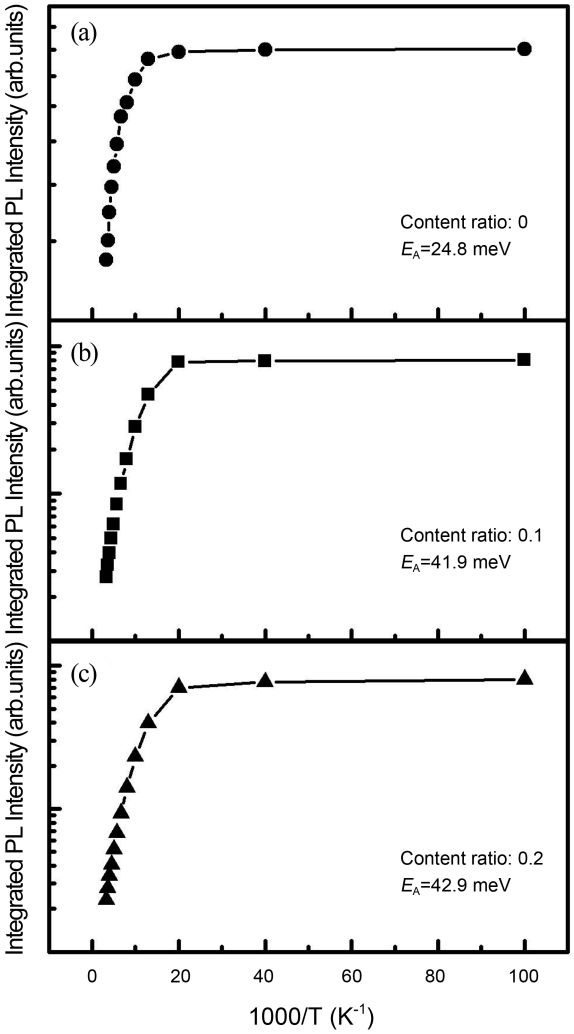

Figure 7. Integrated PL intensity of the $Mg_xZn_{1-x}O$ thin films with the content ratio of (a) 0, (b) 0.1, and (c) 0.2 as a function of the temperature.

by Mg incorporation. For the $Mg_xZn_{1-x}O$ thin films, the shift of the DLE peak is presumably due to the Mg-related trap level. However, detail mechanisms are still not fully understood.

The temperature dependence of the integrated PL intensity for the $Mg_xZn_{1-x}O$ thin films with the various content ratio as a function of the temperature ranging from 10 to 300 K. With increase in the temperature, the PL intensity corresponding to the emission peak is given by

$$I = \frac{I_0}{[1 + C\exp(-\Delta E_A / k_B T)]} \quad (5)$$

where I is the integrated PL intensity, I_0 is the PL intensity at 0 K, C is the ratio of the thermal escape rate to the radiation recombination rate, E_A is the activation energy, and k_B is the Boltzmann constant. Equation (5) assumes that the dominant mechanism for the PL intensity change with increasing temperature is the thermal activation of carriers. Indeed, the integrated PL intensity is decreased almost exponentially with the activation energy at a given temperature. The activation energy of the $Mg_xZn_{1-x}O$ thin films with the content ratio of 0, 0.1, and 0.2 is found to be about 24.8, 41.9, and 42.9 meV, respectively. The activation energy was increased with increase in the content ratio. Kim *et al.*[33] suggested that the enhanced thermal activation energy of $Mg_xZn_{1-x}O$ films was due to the non-uniform distribution of Mg atoms originating from the different crystal structure. It is implied that a lot of the free excitons in MgZnO thin films could survive at RT.[34]

Conclusion

The structural and optical properties of the $Mg_xZn_{1-x}O$ thin films with the various content ratio grown by sol-gel spin-coating method were investigated. The $Mg_xZn_{1-x}O$ thin films exhibit island growth and the grain size was increased with content ratio. However, at the content ratio above 0.2, MgO particles with cubic structure were formed on the surface of the $Mg_xZn_{1-x}O$ thin films, indicating that the Mg content exceeded its solubility limit in the thin films. The limit of the Mg mole fraction of the $Mg_xZn_{1-x}O$ thin films is about 4.7% because the sol-gel spin-coating method is performed under equilibrium nature of crystal growth. The residual stress of the $Mg_xZn_{1-x}O$ thin films is increased with increase in the Mg mole fraction. PL revealed blue-shift in NBE peak and increase in activation energy, as the Mg mole fraction of the $Mg_xZn_{1-x}O$ thin films increased.

Acknowledgments. This research was supported by Basic Science Research Program through the National Research Foundation of Korea (NRF) funded by the Ministry of Education, Science and Technology (No. 2011-0003067).

References

1. Wang, Y.-L.; Kim, H. S.; Norton, D. P.; Pearton, S. J.; Ren, F. *Appl. Phys. Lett.* **2008**, *92*, 112101.
2. Kim, H. S.; Lugo, F.; Pearton, S. J.; Norton, D. P.; Wang, Y.-L.; Ren, F. *Appl. Phys. Lett.* **2008**, *92*, 112108.
3. Lin, S. S.; Lu, J. G.; Ye, Z. Z.; He, H. P.; Gu, X. Q.; Chen, L. X.; Huang, J. Y.; Zhao, B. H. *Solid State Commun.* **2008**, *148*, 25.
4. Hwang, D.-K.; Oh, M.-S.; Lim, J.-H.; Park, S.-J. *J. Phys. D*: *Appl. Phys.* **2007**, *40*, R387.
5. Pan, X.; Li, J.; Zeng, Y.; Gu, X.; Zhu, L.; Zhao, B.; Che, Y. *Appl. Surf. Sci.* **2007**, *253*, 6060.
6. Shim, H. S.; Han, N. S.; Seo, J. H.; Park, S. M.; Song, J. K. *Bull. Korean Chem. Soc.* **2010**, *31*, 2675.
7. Zhang, X. L.; Chua, S. J.; Yong, A. M.; Yang, H. Y.; Lau, S. P.; Yu, S. F.; Sun, X. W.; Miao, L.; Tanemura, M.; Tanemura, S. *Appl. Phys. Lett.* **2007**, *90*, 013107.
8. Cong, C. X.; Yao, B.; Xing, G. Z.; Xie, Y. P.; Guan, L. X.; Li, B. H.; Wang, X. H.; Wei, Z. P.; Zhang, Z. Z.; Lv, Y. M.; Shen, D. Z.; Fan, X. W. *Appl. Phys. Lett.* **2006**, *89*, 262108.
9. Shibata, H.; Tampo, H.; Matsubara, K.; Yamada, A.; Sakurai, K.; Ishizuka, S.; Niki, S.; Sakai, M. *Appl. Phys. Lett.* **2007**, *90*, 124104.
10. Choopun, S.; Vispute, R. D.; Yang, W.; Sharma, R. P.; Venkatesan, T.; Shen, H. *Appl. Phys. Lett.* **2002**, *80*, 1529.
11. Shrestha, S. P.; Ghimire, R.; Nakarmi, J. J.; Kim, Y.-S.; Shrestha, S.; Park, C.-Y.; Boo, J.-H. *Bull. Korean Chem. Soc.* **2010**, *31*, 112.
12. Zhao, D. X.; Liu, Y. C.; Shen, D. Z.; Lu, Y. M.; Zhang, J. Y.; Fan,

X. W. *J. Cryst. Growth* **2002**, *234*, 427.
13. Ohtomo, A.; Kawasaki, M.; Koida, T.; Masubuchi, K.; Koinuma, H.; Sakurai, Y.; Toshida, Y.; Yasuda, T.; Segawa, Y. *Appl. Phys. Lett.* **1998**, *72*, 2466.
14. Yang, W.; Hullavarad, S. S.; Nagaraj, B.; Takeuchi, I.; Sharma, R. P.; Venkatesan, T.; Vispute, R. D.; Shen, H. *Appl. Phys. Lett.* **2003**, *82*, 3424.
15. Chen, N. B.; Sui, C. H. *Mat. Sci. Eng. B* **2006**, *126*, 16.
16. Tsukazaki, A.; Ohtomo, A.; Kawasaki, M.; Makino, T.; Chia, C. H.; Segawa, Y.; Koinuma, H. *Appl. Phys. Lett.* **2004**, *84*, 3858.
17. Hullavarad, S. S.; Dhar, S.; Varughese, B.; Takeuchi, I.; Venkatesan, T.; Vispute, R. D. *J. Vac. Sci. Technol. A* **2005**, *23*, 982.
18. Chakrabarti, S.; Kar, S.; Dev, A.; Chaudhuri, S. *Phys. Stat. Sol. (a)* **2005**, *202*, 441.
19. Cho, M. Y.; Kim, M. S.; Choi, H. Y.; Jeon, S. M.; Kim, G. S.; Kim, D. Y.; Yim, K. G.; Lee, D.-Y.; Kim, J. S.; Kim, J. S.; Lee, J. I.; Leem, J.-Y. *J. Korean Phys. Soc.* **2010**, *56*, 1833.
20. Shujun, Z.; Jiguo, Z.; Zhenxiang, C.; Guangyoung, Z.; Jianru, H.; Huanchu, C. *J. Cryst. Growth* **1999**, *203*, 186.
21. Murakawa, T.; Fukudome, T.; Hayashi, T.; Isshiki, H.; Kimura, T. *Phys. Stat. Sol. (c)* **2004**, *1*, 2564.
22. Choi, H. Y.; Kim, M. S.; Cho, M. Y.; Kim, G. S.; Jeon, S. M.; Yim, K. G.; Kim, D. Y.; Ryu, H. H.; Lee, D.-Y.; Kim, J. S.; Kim, J. S.; Son, J.-S.; Lee, J. I.; Leem, J.-Y. *J. Korean Phys. Soc.* **2010**, *56*, 1514.
23. Lee, H.-Y.; Wang, M.-Y.; Chang, K.-J.; Lin, W.-J. *IEEE Photonic. Tech. L.* **2008**, *20*, 2108.
24. You, J. B.; Zhang, X. W.; Dong, J. J.; Song, X. M.; Yin, Z. G.; Chen, N. F.; Yan, H. *Nanoscale Res. Lett.* **2009**, *4*, 1121.
25. Zhu, L.; Zhi, M,; Ye, Z, Zhao, B. *Appl. Phys. Lett.* **2006**, *88*, 113106.
26. Wang, C.; Zhan, P.; Yue, J.; Zhang, Y.; Zheng, L. *Physca B* **1997**, *403*, 459.
27. Ghosh, R.; Basak, D. *J. Appl. Phys.* **2007**, *101*, 023507.
28. Zhang, S. B.; Wei, S. H.; Zunger, A. *Phys. Rev. B* **2001**, *63*, 075205.
29. Tuomisto, F.; Saarinen, K.; Look, D. C.; Farlow, G. C. *Phys. Rev. B* **2006**, *72*, 085206.
30. Guo, B.; Qiu, Z. R.; Wong, K. S. *Appl. Phys. Lett.* **2003**, *82*, 2290.
31. Trunk, M.; Venkatachalapathy, V.; Galeckas, A.; Kuznetsov, A. Y. *Appl. Phys. Lett.* **2010**, *97*, 211901.
32. Ogawa, Y.; Fujihara, S. *J. Electrochem. Soc.* **2007**, *154*, J283.
33. Kim, Y. Y.; Kong, B. H,; Choi, M. K.; Cho, H. K. *Mater. Sci. Eng. B-Adv.* **2009**, *165*, 80.
34. Pan, C.-J.; Lin, K.-F.; Hsu, W.-T.; Hsieh, W.-F. *J. Appl. Phys.* **2007**, *102*, 123504.